

Description of ^8Be as Deformed Gas-like Two-Alpha-Particle States

Yasuro FUNAKI¹, Hisashi HORIUCHI¹, Akihiro TOHSAKI²,
Peter SCHUCK³, and Gerd RÖPKE⁴

¹ *Department of Physics, Kyoto University, Kyoto 606-8502, Japan*

² *Department of Fine Materials Engineering, Shinshu University,
Ueda 386-8567, Japan*

³ *Institut de Physique Nucleaire, 91406 Orsay Cedex, France*

⁴ *FB Physik, Universität Rostock, D-18051 Rostock, Germany*

(Received)

In order to study non-zero spin excitations of the recently proposed α -cluster condensation in the self-conjugate $4n$ nuclei, spatial deformation is introduced into the model wave function of the α -cluster condensate. The rotational band states of ^8Be are investigated as a first step of a test case for the study of the deformation of the α -cluster condensate. Calculations reproduce well the binding energy of the 0^+ ground state and also the excitation energy of the 2^+ state. Our 0^+ wave function is found to be almost exactly equal to the 0^+ wave function obtained by the generator coordinate method using Brink's 2α wave function. The study shows that both the 0^+ ground and 2^+ excited states can be considered as having a gas-like (i.e. weakly bound) 2α -cluster structure. As for the 0^+ ground state, the change of the wave function, due to the introduction of the deformation, is found to be very small.

§1. Introduction

Recently we presented a conjecture that near the $n\alpha$ threshold in self-conjugate $4n$ nuclei there exist excited states of dilute density which are composed of a weakly interacting gas of alpha particles and which can be considered as an $n\alpha$ condensed state¹⁾. This conjecture was examined in ^{12}C and ^{16}O by using a new α -cluster wave function of the α -particle condensate type. The second 0^+ state in ^{12}C near the 3α threshold was interpreted as such a condensed state as well as the fifth 0^+ T=0 state in ^{16}O near the 4α -particle threshold.

The new α -cluster wave function of the α -particle condensate type which we used in our previous study is an eigen state of zero angular momentum and represents a condensation of α -particles in a spherically symmetric state. Therefore this new α -cluster wave function can describe only states of zero angular momentum. On the other hand, in ^{12}C there exist some excited states above the 3α threshold which have non-zero angular momenta and are considered to have well-developed 3α cluster structure²⁾. Actually many microscopic 3α cluster model calculations gave the result that not only the second 0^+ state near the 3α threshold but also some excited states with non-zero spin above the 3α threshold have 3α structure of dilute density³⁾. The question then arises whether we can identify some excitation modes of the α -cluster condensate with those excited states.

As a possible excitation mode of the α -cluster condensate we can of course

consider partial breaking of the condensate like that due to the promotion of one α -cluster from the condensed s -orbit to a higher-lying orbit with non-zero spin. As another possibility for the excitation mode we can consider spatial deformation of the α -cluster condensate. If the deformation is not energetically stable, we can expect vibrational excitations around the spherical shape, while if the deformation is stable, we can expect the appearance of rotational excitations.

The purpose of the present paper is to study the possibility of spatial deformation of the α -cluster condensate. This study is made in introducing a wave function of the α -cluster condensate with deformation which is obtained by a natural modification of our previous wave function of the spherical α -cluster condensate. As a first step for the study of deformation, we investigate the ${}^8\text{Be}$ nucleus. The ground state of ${}^8\text{Be}$ is known to have a well-developed 2α cluster structure with large spatial separation between the two α 's in relative s -state. With only two α -particles this state can hardly be considered as an α -particle condensation, but rather as a weakly bound state of two bosons in relative s -state thus exhibiting a gas-like structure of dilute density. Our wave function of Ref. ¹⁾ is perfectly adapted to also treat only two α 's and it will serve us as a test case to treat more α -particles in the future. The nucleus ${}^8\text{Be}$ is known to have rotational excited states with large α -decay widths Γ_α , namely a 2^+ state at 2.90 MeV with $\Gamma_\alpha = 1.45$ MeV and a 4^+ state at 11.4 MeV with $\Gamma_\alpha \sim 7$ MeV ⁴⁾. We will see that our investigation shows that in ${}^8\text{Be}$ the α -cluster condensed state is deformable and the experimentally observed rotational band can be explained as being generated from the α -cluster condensate with deformation. We will also see that our 0^+ wave function is almost exactly equal to the 0^+ wave function obtained by the generator coordinate method using Brink's 2α wave function.

§2. Deformed α -particle condensate

2.1. Wave function

The wave function of the α -cluster condensate with deformation can be expressed as follows by a slight modification of our previous wave function of the spherical α -cluster condensation:

$$|\Phi_{n\alpha}\rangle = (C_\alpha^\dagger)^n |\text{vac}\rangle, \quad (2.1)$$

where the α -particle creation operator C_α^\dagger in a deformed center of mass orbit is given by

$$C_\alpha^\dagger = \int d^3R \exp\left(-\frac{R_x^2}{\beta_x^2} - \frac{R_y^2}{\beta_y^2} - \frac{R_z^2}{\beta_z^2}\right) \int d^3r_1 \cdots d^3r_4 \\ \times \varphi_{0s}(\mathbf{r}_1 - \mathbf{R}) a_{\sigma_1\tau_1}^\dagger(\mathbf{r}_1) \cdots \varphi_{0s}(\mathbf{r}_4 - \mathbf{R}) a_{\sigma_4\tau_4}^\dagger(\mathbf{r}_4). \quad (2.2)$$

Here

$$\varphi_{0s}(\mathbf{r}) = (\pi b^2)^{-3/4} \exp\left(-\frac{\mathbf{r}^2}{2b^2}\right), \quad (2.3)$$

and $a_{\sigma\tau}^\dagger(\mathbf{r})$ is the creation operator of a nucleon with spin-isospin $\sigma\tau$ at the spatial point \mathbf{r} . Our previous wave function of the spherical α -cluster condensation is just

the case of $\beta_x = \beta_y = \beta_z = R_0$ in Eq.(2.2). The total $n\alpha$ wave function therefore can be written as

$$\begin{aligned} & \langle \mathbf{r}_1 \sigma_1 \tau_1, \dots, \mathbf{r}_{4n} \sigma_{4n} \tau_{4n} | \Phi_{n\alpha} \rangle \\ & \propto \mathcal{A} \left[\exp \left\{ - \sum_{i=1}^n \left(\frac{2X_{ix}^2}{B_x^2} + \frac{2X_{iy}^2}{B_y^2} + \frac{2X_{iz}^2}{B_z^2} \right) \right\} \phi(\alpha_1) \cdots \phi(\alpha_n) \right], \end{aligned} \quad (2.4)$$

where $B_k^2 = b^2 + 2\beta_k^2$, ($k = x, y, z$), and $\mathbf{X}_i = (1/4) \sum_n^4 \mathbf{r}_{in}$ is the center-of-mass coordinate of the i th α -cluster α_i . The internal wave function of the α -cluster α_i is $\phi(\alpha_i) \propto \exp[-(1/2b^2) \sum_n^4 (\mathbf{r}_{in} - \mathbf{X}_i)^2]$. The operator \mathcal{A} is the total antisymmetrizer. It is to be noted that the wave function of Eqs. (2.1) and (2.4) expresses the state where n α -clusters occupy the same deformed center of mass orbit $\exp\{-\frac{2}{B_x^2} X_x^2 + \frac{2}{B_y^2} X_y^2 + \frac{2}{B_z^2} X_z^2\}$, while the intrinsic α -particle wave function stays spherical. We can easily see that the total center-of-mass motion is separated out of the wave function of Eqs.(2.1) and (2.4) because of the relation,

$$\sum_{i=1}^n X_{ik}^2 = nX_{Gk}^2 + \sum_{i=1}^n (X_{ik} - X_{Gk})^2, \quad (k = x, y, z), \quad \mathbf{X}_G \equiv (1/n) \sum_{i=1}^n \mathbf{X}_i. \quad (2.5)$$

The wave function of the α -cluster condensation with deformation expressed by Eqs.(2.1) and (2.4) is a superposition of Brink's α -cluster model wave function, $\Phi^B(\mathbf{R}_1, \dots, \mathbf{R}_n)$,

$$\begin{aligned} & \Phi_{n\alpha}(\beta_x, \beta_y, \beta_z) \equiv \langle \mathbf{r}_1 \sigma_1 \tau_1, \dots, \mathbf{r}_{4n} \sigma_{4n} \tau_{4n} | \Phi_{n\alpha} \rangle \\ & = \int d^3R_1 \cdots d^3R_n \exp \left\{ - \sum_{i=1}^n \left(\frac{R_{ix}^2}{\beta_x^2} + \frac{R_{iy}^2}{\beta_y^2} + \frac{R_{iz}^2}{\beta_z^2} \right) \right\} \Phi^B(\mathbf{R}_1, \dots, \mathbf{R}_n), \end{aligned} \quad (2.6)$$

$$\Phi^B(\mathbf{R}_1, \dots, \mathbf{R}_n) \equiv \det\{\varphi_{0s}(\mathbf{r}_1 - \mathbf{R}_1) \chi_{\sigma_1 \tau_1} \cdots \varphi_{0s}(\mathbf{r}_{4n} - \mathbf{R}_n) \chi_{\sigma_{4n} \tau_{4n}}\}, \quad (2.7)$$

where $\chi_{\sigma\tau}$ is the nucleon spin-isospin wave function. The form of Eq.(2.6) is directly obtained from Eqs.(2.1) \sim (2.3), and the form of Eq.(2.4) can be obtained from Eq.(2.6) using the relation,

$$\begin{aligned} & \frac{1}{\sqrt{4!}} \det\{\varphi_{0s}(\mathbf{r}_1 - \mathbf{R}) \chi_{\sigma_1 \tau_1} \cdots \varphi_{0s}(\mathbf{r}_4 - \mathbf{R}) \chi_{\sigma_4 \tau_4}\} \\ & = \left(\frac{4}{\pi b^2} \right)^{3/4} \exp \left\{ - \frac{2}{b^2} (\mathbf{X} - \mathbf{R})^2 \right\} \phi(\alpha), \end{aligned} \quad (2.8)$$

where $\mathbf{X} = (1/4) \sum_{i=1}^4 \mathbf{r}_i$. An α -condensed wave function with good angular momentum is obtained by projecting out the angular momentum from the deformed α -condensed wave function as

$$\begin{aligned} & \Phi_{n\alpha}^J(\beta_x, \beta_y, \beta_z) = \int d\Omega D_{MK}^{J*}(\Omega) \hat{R}(\Omega) \Phi_{n\alpha}(\beta_x, \beta_y, \beta_z) \\ & = \int d\Omega D_{MK}^{J*}(\Omega) \int d^3R_1 \cdots d^3R_n \exp \left(- \sum_{i=1}^n \sum_{k=x,y,z} \frac{R_{ik}^2}{\beta_k^2} \right) \end{aligned}$$

$$\begin{aligned}
& \times \Phi^B(R^{-1}(\Omega)\mathbf{R}_1, \dots, R^{-1}(\Omega)\mathbf{R}_n), \\
& = \int d\Omega D_{MK}^{J*}(\Omega) \int d^3R_1 \cdots d^3R_n \exp \left\{ - \sum_{i=1}^n \sum_{k=x,y,z} \frac{(R(\Omega)\mathbf{R}_i)_k^2}{\beta_k^2} \right\} \\
& \times \Phi^B(\mathbf{R}_1, \dots, \mathbf{R}_n), \tag{2.9}
\end{aligned}$$

where Ω is the Euler angle, $D_{MK}^J(\Omega)$ is the Wigner D-function, $\widehat{R}(\Omega)$ is the rotation operator, and $R(\Omega)$ is the 3×3 rotation matrix corresponding to $\widehat{R}(\Omega)$. Here use is made of the relation, $\varphi_{0s}(R(\Omega)\mathbf{r} - \mathbf{R}) = \varphi_{0s}(\mathbf{r} - R^{-1}(\Omega)\mathbf{R})$. It is to be noted that the rotation with respect to the total angular momentum is equivalent to the rotation with respect to the total orbital angular momentum, since the intrinsic spins of α -clusters are saturated.

In this paper we only treat the case of axially symmetric deformation taking the z-axis as the symmetry axis; $\beta_x = \beta_y \neq \beta_z$. In this case, we can replace $\int d\Omega$ by $\int d \cos \theta$, $D_{MK}^J(\Omega)$ by $d_{M0}^J(\theta)$, $\widehat{R}(\Omega)$ by $\widehat{R}_y(\theta)$, and $R(\Omega)$ by $R_y(\theta)$. Here $\widehat{R}_y(\theta)$ and $R_y(\theta)$ are the rotation operator and matrix, respectively, representing the rotation by the angle θ around the y-axis.

2.2. Elimination of spurious center-of-mass motion

As already mentioned, the total center-of-mass motion is separated out of the wave function $\Phi_{n\alpha}(\beta_x, \beta_y, \beta_z)$. However, the separation of the total center-of-mass motion is no more true for the angular-momentum-projected wave function $\Phi_{n\alpha}^J(\beta_x, \beta_y, \beta_z)$. Nevertheless the spurious admixture of the the total center-of-mass motion can be removed rather easily, as we explain now.

By using Eq.(2.5) we separate the center-of-mass wave function from $\Phi_{n\alpha}(\beta_x, \beta_y, \beta_z)$ as

$$\Phi_{n\alpha}(\beta_x = \beta_y, \beta_z) = Q \exp \left\{ - \frac{2n}{B_x^2} (X_{Gx}^2 + X_{Gy}^2) - \frac{2n}{B_z^2} X_{Gz}^2 \right\} \widehat{\Phi}_{n\alpha}(\beta_x = \beta_y, \beta_z), \tag{2.10}$$

$$\widehat{\Phi}_{n\alpha}(\beta_x = \beta_y, \beta_z) = \mathcal{A} \left[\exp \left\{ - \sum_{i=1}^n \sum_{k=x,y,z} \frac{2}{B_k^2} (X_{ik} - X_{Gk})^2 \right\} \phi(\alpha_1) \cdots \phi(\alpha_n) \right], \tag{2.11}$$

where Q is some constant number. Clearly $\widehat{\Phi}_{n\alpha}(\beta_x = \beta_y, \beta_z)$ does not contain the center-of-mass coordinate \mathbf{X}_G and is the internal wave function of $\Phi_{n\alpha}(\beta_x = \beta_y, \beta_z)$. The correct α -condensed wave function with good angular momentum is not $\Phi_{n\alpha}^J(\beta_x = \beta_y, \beta_z)$ given in Eq.(2.9) but is $\widehat{\Phi}_{n\alpha}^J(\beta_x = \beta_y, \beta_z)$ defined as

$$\widehat{\Phi}_{n\alpha}^J(\beta_x = \beta_y, \beta_z) = \int d \cos \theta d_{M0}^J(\theta) \widehat{R}_y(\theta) \widehat{\Phi}_{n\alpha}(\beta_x = \beta_y, \beta_z). \tag{2.12}$$

The matrix element of a general translationally invariant scalar operator \widehat{O} with the correct α -condensed wave function $\widehat{\Phi}_{n\alpha}^J(\beta_x = \beta_y, \beta_z)$ is calculated as

$$\frac{\langle \widehat{\Phi}_{n\alpha}^J(\beta_x = \beta_y, \beta_z) | \widehat{O} | \widehat{\Phi}_{n\alpha}^J(\beta_x = \beta_y, \beta_z) \rangle}{\langle \widehat{\Phi}_{n\alpha}^J(\beta_x = \beta_y, \beta_z) | \widehat{\Phi}_{n\alpha}^J(\beta_x = \beta_y, \beta_z) \rangle}$$

$$= \frac{\int d \cos \theta d_{00}^J(\theta) \langle \widehat{\Phi}_{n\alpha}(\beta_x = \beta_y, \beta_z) | \widehat{O} \widehat{R}_y(\theta) | \widehat{\Phi}_{n\alpha}(\beta_x = \beta_y, \beta_z) \rangle}{\int d \cos \theta d_{00}^J(\theta) \langle \widehat{\Phi}_{n\alpha}(\beta_x = \beta_y, \beta_z) | \widehat{R}_y(\theta) | \widehat{\Phi}_{n\alpha}(\beta_x = \beta_y, \beta_z) \rangle}. \quad (2.13)$$

The important technique for the calculation of the matrix elements of the integrands in this expression is to use the following relation

$$\begin{aligned} & \langle \widehat{\Phi}_{n\alpha}(\beta_x = \beta_y, \beta_z) | \widehat{O} \widehat{R}_y(\theta) | \widehat{\Phi}_{n\alpha}(\beta_x = \beta_y, \beta_z) \rangle \\ &= \frac{1}{Q^2 P(\theta)} \langle \Phi_{n\alpha}(\beta_x = \beta_y, \beta_z) | \widehat{O} \widehat{R}_y(\theta) | \Phi_{n\alpha}(\beta_x = \beta_y, \beta_z) \rangle, \end{aligned} \quad (2.14)$$

$$\begin{aligned} P(\theta) &= \langle \exp\left(-\sum_{k=x,y,z} \frac{2n}{B_k^2} X_{Gk}^2\right) | \widehat{R}_y(\theta) | \exp\left(-\sum_{k=x,y,z} \frac{2n}{B_k^2} X_{Gk}^2\right) \rangle \\ &= \sqrt{\left(\frac{\pi}{4n}\right)^3 \frac{B_x^6 B_z^4}{B_x^2 B_z^2 + (1/4)(B_x^2 - B_z^2)^2 \sin^2 \theta}}. \end{aligned} \quad (2.15)$$

This relation holds because the operator \widehat{O} does not depend on the center-of-mass coordinate \mathbf{X}_G . By using this relation we get

$$\begin{aligned} & \frac{\langle \widehat{\Phi}_{n\alpha}^J(\beta_x = \beta_y, \beta_z) | \widehat{O} | \widehat{\Phi}_{n\alpha}^J(\beta_x = \beta_y, \beta_z) \rangle}{\langle \widehat{\Phi}_{n\alpha}^J(\beta_x = \beta_y, \beta_z) | \widehat{\Phi}_{n\alpha}^J(\beta_x = \beta_y, \beta_z) \rangle} \\ &= \frac{\int d \cos \theta d_{00}^J(\theta) \langle \Phi_{n\alpha}(\beta_x = \beta_y, \beta_z) | \widehat{O} \widehat{R}_y(\theta) | \Phi_{n\alpha}(\beta_x = \beta_y, \beta_z) \rangle / P(\theta)}{\int d \cos \theta d_{00}^J(\theta) \langle \Phi_{n\alpha}(\beta_x = \beta_y, \beta_z) | \widehat{R}_y(\theta) | \Phi_{n\alpha}(\beta_x = \beta_y, \beta_z) \rangle / P(\theta)}. \end{aligned} \quad (2.16)$$

The explicit formulas of the matrix elements of the overlap, the kinetic energy, the two-body nuclear force, and the Coulomb force in the case of the ^8Be system are given in the Appendix A. In Appendix B we will show that the integration over the Euler angle θ can be performed analytically.

2.3. Non-zero spin states on the $\beta_x (= \beta_y) = \beta_z$ line

On the $\beta_x (= \beta_y) = \beta_z$ line the intrinsic state $\widehat{\Phi}_{n\alpha}(\beta_x = \beta_y, \beta_z)$ is spherical and it may seem that we do not get non-zero spin states by the angular momentum projection. But we can construct the non-zero spin states even on the $\beta_x (= \beta_y) = \beta_z$ line using angular momentum projection by the following usual limiting procedure: We first construct the non-zero spin state $\widehat{\Phi}_{n\alpha}^J(\beta_x = \beta_y, \beta_z)$ of Eq.(2.12) for $\beta_x (= \beta_y) \neq \beta_z$ by angular momentum projection. Next we normalize this state obtaining the normalized state $\widehat{\Phi}_{n\alpha}^{\text{NJ}}(\beta_x = \beta_y, \beta_z)$,

$$\widehat{\Phi}_{n\alpha}^{\text{NJ}}(\beta_x = \beta_y, \beta_z) = \frac{\widehat{\Phi}_{n\alpha}^J(\beta_x = \beta_y, \beta_z)}{\|\widehat{\Phi}_{n\alpha}^J(\beta_x = \beta_y, \beta_z)\|}, \quad (2.17)$$

where $\|\Phi\|$ denotes the norm of Φ , $\|\Phi\| = \sqrt{\langle \Phi | \Phi \rangle}$. Since $\|\widehat{\Phi}_{n\alpha}^{\text{NJ}}(\beta_x = \beta_y, \beta_z)\| = 1$, there exists the limiting state

$$\lim_{\beta_x \rightarrow \beta_z} \widehat{\Phi}_{n\alpha}^{\text{NJ}}(\beta_x = \beta_y, \beta_z). \quad (2.18)$$

This limiting state is the non-zero spin wave function we adopt on the $\beta_x(= \beta_y) = \beta_z$ line.

Since $\lim_{\beta_x \rightarrow \beta_z} \widehat{\Phi}_{n\alpha}^J(\beta_x = \beta_y, \beta_z) = 0$, the use of $\widehat{\Phi}_{n\alpha}^{NJ}(\beta_x = \beta_y, \beta_z)$ near the limit of $\beta_x = \beta_z$ is not easy with respect to numerical accuracy. Therefore in our present study of the ${}^8\text{Be}$ system, we calculated the matrix elements with $\widehat{\Phi}_{2\alpha}^{NJ}(\beta_x = \beta_y, \beta_z)$ analytically. This was made possible by performing the angular momentum projection analytically. Then the matrix elements with $\widehat{\Phi}_{2\alpha}^{NJ}(\beta_x = \beta_y, \beta_z)$ near and on the $\beta_x(= \beta_y) = \beta_z$ line were obtained without any difficulty in the numerical calculations. Details are explained in Appendix C.

2.4. Microscopic Hamiltonian

The Hamiltonian H we use in this paper is written as

$$H = T - T_G + V_N + V_C, \quad (2.19)$$

where T is the total kinetic energy operator, T_G is the center-of-mass kinetic energy operator, V_N is the effective two-body nuclear force, and V_C is the Coulomb force between protons. Explicit forms of T and T_G are as follows

$$T = \sum_{i=1}^8 \frac{-\hbar^2}{2m} \left(\frac{\partial}{\partial \mathbf{r}_i} \right)^2, \quad T_G = \frac{-\hbar^2}{16m} \left(\frac{\partial}{\partial \mathbf{X}_G} \right)^2. \quad (2.20)$$

As the effective two-body nuclear force, we adopt the force No.1 of Volkov⁵⁾ which has the following form,

$$V_N = \frac{1}{2} \sum_{i \neq j}^8 \{ (1 - M) - MP_\sigma P_\tau \}_{ij} \sum_{n=1}^2 v_n \exp\left(-\frac{r_{ij}^2}{a_n^2}\right). \quad (2.21)$$

The Coulomb force is given as

$$V_C = \frac{1}{2} \sum_{i \neq j}^8 \frac{1 - \tau_{zi}}{2} \frac{1 - \tau_{zj}}{2} \frac{e^2}{r_{ij}}. \quad (2.22)$$

In our previous study of the alpha condensation in ${}^{12}\text{C}$ and ${}^{16}\text{O}$, we used an effective nuclear force named F1 which contains a three-nucleon force in addition to the two-nucleon force⁶⁾. The reason for this was that in both nuclei we treated not only the α -condensed state of dilute density but also the normal-density states including the ground state. Therefore we had to use a nuclear force which has reasonable density-dependent properties. On the other hand, in the present study we treat only the ground band states of ${}^8\text{Be}$, all of which are expected to have a similar value of low density. Therefore we here use a simpler effective nuclear force than in the previous study.

§3. Results

3.1. Energy surface of the intrinsic state

We first calculate the binding energy for the spherical state of ^8Be which has two parameters b and $\beta_x = \beta_y = \beta_z = R_0$. In Fig.1 we give the contour map of the energy surface in the two parameter space, b and $\beta_x = \beta_y = \beta_z$. The binding energy E_α of the single alpha particle which is independent of the Majorana parameter of the force No.1 of Volkov takes its lowest value $E_\alpha = -27.08$ MeV for the size parameter $b = 1.37$ fm. As the strength of the Majorana parameter M of the Volkov force in ^8Be , we adopt $M = 0.56$. It is because with this value of M , the lowest binding energy takes the value -54.33 MeV as seen in Fig.1 which is only about 0.17 MeV lower than the theoretical two-alpha threshold energy, $2E_\alpha = -54.16$ MeV, in agreement with the experimental binding energy from the two-alpha threshold energy, about + 0.1 MeV. The value of the b parameter at the energy minimum is $b = 1.36$ fm which is very close to but slightly smaller* than the b value of the free alpha particle. It is known that this combination of the values of b and M which are close to $b= 1.37$ fm and $M=0.56$, respectively, gives a very good reproduction of the α - α scattering phase shifts within the framework of the resonating group method⁸⁾.

The qualitative feature of this map is similar to the corresponding maps in ^{12}C and ^{16}O given in our previous paper¹⁾. This map shows a valley running from the outer region with large value of $\beta_x = \beta_y = \beta_z > 10$ fm and $b \approx 1.36$ fm. The valley has a saddle point at $\beta_x = \beta_y = \beta_z \approx 8.5$ fm. Beyond the saddle point the binding energy is almost equal to $2E_\alpha$. The height of the saddle point measured from the theoretical threshold energy, $2E_\alpha$, is about 0.56 MeV. The reason of the appearance of the saddle point is the same in the cases of ^{12}C and ^{16}O and is attributed to the increase of the Coulomb energy and kinetic energy towards the inward direction which around the saddle point region is not yet compensated by the gain in nuclear potential energy. The minimum of the energy surface is located at $\beta_x = \beta_y = \beta_z \approx 3$ fm.

The result that the α -condensed wave function reproduces well the experimental binding energy implies that the ground state of ^8Be can be considered as a 2α -particle s -wave quasi-bound state with a "gas-like" structure of dilute density. By "gas-like" we mean that the state is weakly bound and spreads widely forming a dilute density state and constituent clusters move rather freely.

By fixing the b parameter to $b = 1.36$ fm, which is the b value at the energy minimum of Fig.1, we now calculate the energy of the deformed states. Fig.2 is the contour map of the energy surface in the two parameter space, $\beta_x (= \beta_y)$ and β_z . This figure shows that the energy minimum lies on the $\beta_x = \beta_z$ line, which means that the energy minimum is attained for the spherical shape. However, it is well known that nuclear deformation can not be deduced from a calculation without angular momentum projection. That is, we often encounter the case where the energy of the angular-momentum-projected state has a minimum for non-zero deformation although the energy of the intrinsic state without angular momentum projection

* This smaller b -value may be interpreted as an effect of the Pauli-principle:one way to minimise the repulsive effect of antisymmetrisation is that the clusters make themselves smaller. This is clearly seen in the case of a low density gas of deuterons as explained in Ref.⁷⁾

favors a spherical shape.

3.2. Energy surfaces of spin-projected states

In Fig.3 we show the contour map of the energy surface corresponding to the spin-projected states $J^\pi = 0^+$ in the two parameter space, $\beta_x (= \beta_y)$ and β_z . Now we see that the energy minimum no more lies on the $\beta_x = \beta_z$ line but is located at $\beta_x (= \beta_y) \approx 1.8$ fm and $\beta_z \approx 7.8$ fm in the prolate region of the map. The value of the energy minimum of -54.45 MeV means that the energy gain from angular momentum projection is only about 0.12 MeV. Reflecting this small energy gain, there is a valley with an almost flat bottom running through this energy minimum to the second energy minimum at $\beta_x (= \beta_y) \approx 4.1$ fm and $\beta_z \approx 0.0$ fm in the oblate region of the map. The bottom line of this valley crosses the $\beta_x = \beta_z$ line at $\beta_x = \beta_z = 3$ fm which is just the energy minimum of Fig.2 for the spherical α -condensed state. The variation of the binding energy along the bottom line of the valley is less than 0.12 MeV.

How much different are the spin-projected wave functions along the bottom line of the valley from one another? The squared overlap $|\langle \hat{\Phi}_I^{0+} | \hat{\Phi}_{II}^{0+} \rangle|^2$ of the normalized wave function $\hat{\Phi}_I^{0+}$ at the energy minimum and the normalized wave function $\hat{\Phi}_{II}^{0+}$ at $\beta_x = \beta_z = 3$ fm is about 0.98. This implies that $\hat{\Phi}_I^{0+}$ is almost equivalent to $\hat{\Phi}_{II}^{0+}$. We also calculated the squared overlap $|\langle \hat{\Phi}_I^{0+} | \hat{\Phi}_{III}^{0+} \rangle|^2$ of $\hat{\Phi}_I^{0+}$ at the energy minimum and the normalized wave function $\hat{\Phi}_{III}^{0+}$ at the second energy minimum. The value of $|\langle \hat{\Phi}_I^{0+} | \hat{\Phi}_{III}^{0+} \rangle|^2$ is about 0.99. This result implies that $\hat{\Phi}_I^{0+}$ in the prolate region is almost equivalent to $\hat{\Phi}_{III}^{0+}$ in the oblate region. Hence we can say that the 0^+ component contained in the deformed intrinsic state along the bottom line of the valley is almost unchanged and is almost equivalent to the spherical condensed state at $\beta_x = \beta_z = 3$ fm which is the energy minimum of Fig.2.

In Fig.4 (a) we show the squared overlap $O(\beta_x, \beta_z) = |\langle \hat{\Phi}_{2\alpha}^{N0+}(\beta_x, \beta_z) | \hat{\Phi}_I^{0+} \rangle|^2$ in the form of the contour map in the two parameter space, $\beta_x (= \beta_y)$ and β_z , where $\hat{\Phi}_{2\alpha}^{N0+}(\beta_x, \beta_z)$ is the normalized wave function of $\hat{\Phi}_{2\alpha}^{0+}(\beta_x = \beta_y, \beta_z)$ of Eq.(2.12). The feature of the contour map of Fig.4 (a) is rather similar to the contour map of Fig.3.

Now we show in Fig.5 the contour map of the energy surface for the spin-projected states to $J^\pi = 2^+$ in the two parameter space, $\beta_x (= \beta_y)$ and β_z . Unlike the 0^+ case, we see no local minimum. The binding energy becomes deeper as β_x or β_z becomes larger. Let us consider the region between two lines, $\beta_x + \beta_z \approx 3$ fm and $\beta_x + \beta_z \approx 7$ fm. The line, $\beta_x + \beta_z \approx 3$ fm, is just the beginning of the energetically steeply-rising region towards $\beta_x = \beta_z = 0$. The line, $\beta_x + \beta_z \approx 7$ fm, is approximately the boarder of the interaction region of two alpha particles. The region between the two lines, $\beta_x + \beta_z \approx 3$ fm and $\beta_x + \beta_z \approx 7$ fm is rather flat in energy, that is the binding energy in this region lies approximately between -51.0 MeV and -51.8 MeV. The height of this plateau region measured from the 0^+ energy minimum, -54.45 MeV, is approximately between 2.65 MeV and 3.45 MeV. Although, without imposing the correct boundary condition of the resonance, we cannot make a definite statement, we can safely conjecture that we will have a 2^+ resonance of the excitation energy between 2.65 MeV and 3.45 MeV. This excitation energy is in good agreement with

the experimental 2^+ excitation energy at 2.9 MeV. The reason of our conjecture is as follows. Let us make the strength of the Majorana exchange mixture M slightly smaller, taking $M=0.56$ instead of $M=0.54$. The contour map of the $J^\pi = 2^+$ energy surface for $M=0.54$ is shown in Fig.6. The feature of the contour map of Fig.6 is very similar to that of Fig.5, but we now have a local minimum at $\beta_x(=\beta_y) \approx 3.9$ fm and $\beta_z \approx 0.0$ fm in the oblate region of the map. The binding energy of this local minimum is -52.28 MeV. We show in Fig.7 the contour map of the $J^\pi = 0^+$ energy surface for the same $M=0.54$. The feature of the contour map of Fig.7 is very similar to that of Fig.3 with $M=0.56$ and the energy minimum which is slightly deeper than that of Fig.3 is now at -55.19 MeV. Then the excitation energy of the 2^+ state is 2.91 MeV. This value of the 2^+ excitation energy is very close to the experimental 2^+ excitation energy of 2.9 MeV.

In Fig.4 (b) we show the squared overlap $O(\beta_x, \beta_z) = |\langle \hat{\Phi}_{2\alpha}^{\text{N}2^+}(\beta_x, \beta_z) | \hat{\Phi}_1^{2^+} \rangle|^2$ in the form of the contour map in the two parameter space, $\beta_x(=\beta_y)$ and β_z , where $\hat{\Phi}_{2\alpha}^{\text{N}2^+}(\beta_x, \beta_z)$ is the normalized wave function of $\hat{\Phi}_{2\alpha}^{2^+}(\beta_x = \beta_y, \beta_z)$ of Eq.(2.12), and $\hat{\Phi}_1^{2^+}$ is the normalized wave function of the energy minimum of Fig.6, $\beta_x(=\beta_y) \approx 3.9$ fm and $\beta_z \approx 0.0$ fm. This figure shows that the 2^+ wave function is almost unchanged from $\hat{\Phi}_1^{2^+}$ along the valley running from this energy minimum in the oblate region deeply into the region of prolate deformation. Hence we can say that the 2^+ component contained in the deformed intrinsic state along this bottom line of the valley is almost unchanged.

We also checked the cases of $M < 0.54$ for the 2^+ -state and again found the existence of a local minimum. The excitation energy of the 2^+ state at the local minimum was found to be around 2.9 MeV.

From the above results for the 0^+ and 2^+ states, in using the deformed 2α -state, we reach two conclusions: (1) For the 0^+ state, the introduction of the deformed 2α -state plays essentially no role and the description with the spherical 2α -state is justified. (2) The deformed 2α -state yields a nice description of the 2^+ state, which gives us a new understanding about the character of the 2^+ state. Namely the 2^+ state can be considered to be a gas-like state of 2α -particles in a relative d -wave. The merit of the introduction of the deformed 2α -state is just this point. That is, we have obtained the picture about ^8Be that not only the ground state but also the excited 2^+ state can be interpreted in terms of a gas-like 2α -structure. This conclusion encourages us to introduce the deformed wave function of the α -condensation in ^{12}C and heavier self-conjugate $4n$ nuclei for a future study of the non-zero spin excitations of α -condensate states.

Let us now study the 4^+ state. Fig.8 shows the contour map of the energy surface corresponding to the spin-projected states of $J^\pi = 4^+$ in the two parameter space, $\beta_x(=\beta_y)$ and β_z . Like the 2^+ case there is no local minimum. We checked the cases of smaller M values than 0.56 including 0.54 but we found no local minimum in all cases. In Fig.8 we see that the approximately flat region of the 4^+ surface is slightly pulled into a smaller $\beta_x + \beta_z$ region compared to the case of the 2^+ energy surface. The binding energy in the region between the two lines, $\beta_x + \beta_z \approx 2$ fm and $\beta_x + \beta_z \approx 4$ fm, lies approximately between -42 MeV and -45 MeV, which in terms of the excitation

energy is between 9.45 MeV and 12.45 MeV. Although this excitation energy region between 9.45 MeV and 12.45 MeV is near the experimental 4^+ excitation energy, 11.4 MeV, we need more careful calculation including the resonance boundary condition in order to get reliable conclusion about the 4^+ resonance.

In this context it is useful to mention the calculation of the energy curve of ^8Be using Brink's 2α wave function. The energy curve is the binding energy as a function of the inter- α distance R . The energy curve for the 2^+ resonance has a local minimum inside the interaction region with $R < 6$ fm, while that for the 4^+ resonance does not have any local minimum.

3.3. Comparison with the solution of the 2α Hill-Wheeler equation

The wave function of the 2α -condensed state belongs to the functional space spanned by the wave functions of the following form,

$$\mathcal{A}\{\chi(\mathbf{r})\phi(\alpha_1)\phi(\alpha_2)\}, \quad (3.1)$$

with $\chi(\mathbf{r})$ representing an arbitrary function. Here \mathbf{r} is the relative coordinate between two α clusters, $\mathbf{r} = \mathbf{X}_1 - \mathbf{X}_2$. The diagonalization of the Hamiltonian within this functional space is accomplished just by solving the well-known equation of the resonating group method (RGM),

$$\langle\phi(\alpha_1)\phi(\alpha_2)|(H - E)|\mathcal{A}\{\chi(\mathbf{r})\phi(\alpha_1)\phi(\alpha_2)\}\rangle = 0. \quad (3.2)$$

The solution of this RGM equation is equivalent to the solution of the 2α Hill-Wheeler equation,

$$\int d^3R \langle\Phi^B\left(\frac{1}{2}\mathbf{S}, -\frac{1}{2}\mathbf{S}\right)|(H - E)|\Phi^B\left(\frac{1}{2}\mathbf{R}, -\frac{1}{2}\mathbf{R}\right)\rangle f(\mathbf{R}) = 0. \quad (3.3)$$

Our wave functions of 2α -condensation are approximations to the RGM wave functions $\mathcal{A}\{\chi(\mathbf{r})\phi(\alpha_1)\phi(\alpha_2)\}$ obtained by solving Eq.(3.2) in imposing wave functions of Gaussian shapes. Since the numerical solution of the 2α RGM equation of Eq.(3.2) is not difficult with present-day computers, one may ask why we discuss approximations to the RGM wave functions. The answer is of course obvious: Our study in this paper is to extract and elucidate the α -condensation character of the ^8Be states which the RGM study of ^8Be until now has not clarified even though it has given numerical values of the ^8Be wave functions. Furthermore our present study of the ^8Be states is made in the scope which is not restricted only to the ^8Be states but extends to excited states of general self-conjugate $4n$ nuclei which are of dilute density and are expected to exist near the $n\alpha$ breakup threshold. For the self-conjugate $4n$ nuclei, heavier than ^8Be , especially for their excited states with dilute density, it is no longer easy but very difficult, especially for $n \geq 4$, to solve the RGM equation of motion,

$$\langle\phi(\alpha_1)\cdots\phi(\alpha_n)|(H - E)|\mathcal{A}\{\chi(\boldsymbol{\xi}_1, \cdots, \boldsymbol{\xi}_{n-1})\phi(\alpha_1)\cdots\phi(\alpha_n)\}\rangle = 0, \quad (3.4)$$

where $\boldsymbol{\xi}_1, \cdots, \boldsymbol{\xi}_{n-1}$ are the relative coordinates between $n\alpha$ clusters.

For 0^+ , we solved the 2α Hill-Wheeler equation of Eq.(3.3) and compared the solution with our wave function $\widehat{\Phi}_1^{0^+}$. The Hill-Wheeler equation was solved by discretizing the radial integration as follows

$$\sum_j \langle \Phi^{B0^+}(R_i) | (H - E) | \Phi^{B0^+}(R_j) \rangle f(R_j) = 0,$$

$$\Phi^{B0^+}(R) \equiv \int d^2 \widehat{R} \Phi^B\left(\frac{1}{2}\mathbf{R}, -\frac{1}{2}\mathbf{R}\right), \quad (3.5)$$

where \widehat{R} is the polar angle of \mathbf{R} . The energy expectation value of $\Phi^{B0^+}(R)$ as a function of R , $\langle \Phi^{B0^+}(R) | H | \Phi^{B0^+}(R) \rangle / \langle \Phi^{B0^+}(R) | \Phi^{B0^+}(R) \rangle$, takes its minimum at $R = 3.45$ fm with the minimum energy -52.069 MeV. It should be noted that this value is higher than the energy (-54.448 MeV) of $\widehat{\Phi}_1^{0^+}$ by 2.379 MeV, which is a rather large value. By adopting $R_j = 0.5 \times j$ fm with $j = 1 \sim 23$, we obtained -54.444 MeV as the lowest eigen energy, and the squared overlap of the corresponding wave function with our wave function $\widehat{\Phi}_1^{0^+}$ is 0.9973. When we adopt one more mesh point as $R_j = 0.5 \times j$ fm with $j = 1 \sim 24$, we obtained -54.446 MeV as the lowest eigen energy, and the squared overlap of the corresponding wave function with our wave function $\widehat{\Phi}_1^{0^+}$ becomes 0.9980. We can say that we have obtained almost converged value for the lowest eigen energy of the Hill-Wheeler equation. In principle, the lowest eigen energy of the Hill-Wheeler equation of Eq.(3.5) should be lower than the energy of $\widehat{\Phi}_1^{0^+}$. But the above values of the lowest eigen energy are still slightly higher than the energy of $\widehat{\Phi}_1^{0^+}$. From this result we can say that our wave function $\widehat{\Phi}_1^{0^+}$ is almost exactly equal to the wave function of the lowest energy solution of the Hill-Wheeler equation. This conclusion is surprising but it clearly shows that our model wave function $\widehat{\Phi}_{2\alpha}^{N0^+}(\beta_x = \beta_y, \beta_z)$ is very much suited to the ground state of ^8Be which is a threshold state with dilute density. We can say that this conclusion strongly supports our new picture of the ^8Be structure as a very dilute gas-like structure of 2 α -particles rather than a dumb-bell structure of 2 α -particles.

§4. Discussion

Our study in this paper is based on the use of the spin-projected state $\widehat{\Phi}_{2\alpha}^J(\beta_x = \beta_y, \beta_z)$ obtained from the deformed intrinsic state $\widehat{\Phi}_{2\alpha}(\beta_x = \beta_y, \beta_z)$. Our deformed intrinsic state $\widehat{\Phi}_{2\alpha}(\beta_x = \beta_y, \beta_z)$ is characterized as having a gas-like 2α -structure, i.e. a weakly bound 2α -state. However, in order to be able to impose the same character to the spin-projected state $\widehat{\Phi}_{2\alpha}^J(\beta_x = \beta_y, \beta_z)$, it is necessary that the spin-projected state $\widehat{\Phi}_{2\alpha}^{NJ}(\beta_x = \beta_y, \beta_z)$ is contained in the intrinsic state $\widehat{\Phi}_{2\alpha}^N(\beta_x = \beta_y, \beta_z)$ with non-negligible amplitude, where $\widehat{\Phi}_{2\alpha}^{NJ}(\beta_x = \beta_y, \beta_z)$ and $\widehat{\Phi}_{2\alpha}^N(\beta_x = \beta_y, \beta_z)$ are the normalized states of $\widehat{\Phi}_{2\alpha}^J(\beta_x = \beta_y, \beta_z)$ and $\widehat{\Phi}_{2\alpha}(\beta_x = \beta_y, \beta_z)$, respectively. Therefore we have calculated the magnitude of the squared overlap amplitude, $|\langle \widehat{\Phi}_{2\alpha}^{NJ}(\beta_x = \beta_y, \beta_z) | \widehat{\Phi}_{2\alpha}^N(\beta_x = \beta_y, \beta_z) \rangle|^2$, for $J = 0 \sim 4$, and the results are given in Figs.9 (a) ~ (c) in the form of the contour map in the two parameter space, $\beta_x (= \beta_y)$ and β_z . We see that the minimum-energy states $\widehat{\Phi}_1^{0^+}$ and $\widehat{\Phi}_1^{2^+}$ have strong overlap with their respective intrinsic states.

The energy surfaces given in Figs.3 and 5 are fairly flat. But at the same time we see in Figs.4 (a) and (b) that the wave functions in the energetically flat region are very similar to one another. Therefore the flatness of the energy surface does not imply the appearance of the low-energy excited states. Also the superposition of the wave functions by solving the Hill-Wheeler equation will result in only a slight change of the energy and wave function from the energy and wave function at the energy minimum of the energy surface, respectively.

As explained in § 2.3, the non-zero spin states on the $\beta_x = \beta_z$ line were constructed by the limiting procedure and the matrix elements of these limiting states were calculated analytically. As is seen in the maps of Figs. 5, 6, and 8, the contour lines cross the $\beta_x = \beta_z$ line smoothly with no singular behavior near the $\beta_x = \beta_z$ line. In Fig.10 we show the binding energy of the 2^+ state along the the $\beta_x = \beta_z$ line in the case of $M = 0.56$.

In Fig.4(a) we saw that the minimum-energy 0^+ wave function which is projected out from the prolate intrinsic state is almost the same as the second-minimum-energy 0^+ wave function which is projected out from the oblate intrinsic state. Similarly we saw in Fig.4(b) that the 2^+ wave function which gives the local energy minimum and which is projected out from the oblate intrinsic state is almost the same as the 2^+ wave functions which are projected out from the prolate intrinsic states. These results look very strange at first sight. In order to check whether the prolate intrinsic state is very different from the oblate intrinsic state or not, we calculated the overlap between the intrinsic wave function $\widehat{\Phi}_1$ at the energy minimum for 0^+ which has prolate deformation with the general intrinsic state $\widehat{\Phi}_{2\alpha}(\beta_x = \beta_y, \beta_z)$ including the intrinsic wave function of the second energy minimum which has oblate deformation. In Fig.11 we show the squared overlap $|\langle \widehat{\Phi}_{2\alpha}^N(\beta_x, \beta_z) | \widehat{\Phi}_1^N \rangle|^2$ in the form of a contour map in the two parameter space, $\beta_x (= \beta_y)$ and β_z , where $\widehat{\Phi}_{2\alpha}^N(\beta_x, \beta_z)$ is the normalized wave function of $\widehat{\Phi}_{2\alpha}(\beta_x = \beta_y, \beta_z)$ and $\widehat{\Phi}_1^N$ is the normalized wave function of $\widehat{\Phi}_1$. We see that the overlaps between the prolate intrinsic state $\widehat{\Phi}_1^N$ and the oblate intrinsic states near the second energy minimum are very small. Below, we explain the reason why we have such seemingly strange results for the spin-projected states and indicate that this is due to the simplicity or the smallness of the functional space of the 2α system. The intrinsic wave function of our model which has the form of Eq.(2.11) with $n = 2$ is written as

$$\begin{aligned} \widehat{\Phi}_{2\alpha}(\beta_x = \beta_y, \beta_z) &= \mathcal{A} \left\{ \exp\left(-\frac{r_x^2 + r_y^2}{B_x^2} - \frac{r_z^2}{B_z^2}\right) \phi(\alpha_1) \phi(\alpha_2) \right\}, \\ r_k &\equiv X_{1k} - X_{2k}, \quad (k = x, y, z). \end{aligned} \quad (4.1)$$

The relative wave function $\exp\{- (r_x^2 + r_y^2)/B_x^2 - r_z^2/B_z^2\}$ can be expanded as follows

$$\begin{aligned} \exp\left(-\frac{r_x^2 + r_y^2}{B_x^2} - \frac{r_z^2}{B_z^2}\right) &= \exp\left\{ -\left(\frac{2}{3B_x^2} + \frac{1}{3B_z^2}\right)r^2 - \left(\frac{1}{3B_z^2} - \frac{1}{3B_x^2}\right)(2r_z^2 - r_x^2 - r_y^2) \right\} \\ &= \exp\left\{ -\left(\frac{2}{3B_x^2} + \frac{1}{3B_z^2}\right)r^2 \right\} - \left(\frac{1}{3B_z^2} - \frac{1}{3B_x^2}\right) \sqrt{\frac{16\pi}{5}} r^2 \exp\left\{ -\left(\frac{2}{3B_x^2} + \frac{1}{3B_z^2}\right)r^2 \right\} Y_{20}(\hat{r}) \\ &+ \dots, \end{aligned} \quad (4.2)$$

where \hat{r} is the polar angle of $\mathbf{r} = \mathbf{X}_1 - \mathbf{X}_2$. The sign of the coefficient of the second term, $(1/3B_z^2 - 1/3B_x^2)$, is opposite for prolate and oblate deformations, and it makes the overlap between prolate and oblate intrinsic states small. However once we project out the good spin state, the situation changes strongly. For the 0^+ -state, the projected wave function has the same following form for the leading term

$$\mathcal{A}\left[\exp\left\{-\left(\frac{2}{3B_x^2} + \frac{1}{3B_z^2}\right)r^2\right\}\phi(\alpha_1)\phi(\alpha_2)\right], \quad (4.3)$$

irrespectively of the deformation of its original intrinsic state. Similarly for 2^+ , the projected wave function has the same following form for the leading term

$$\mathcal{A}\left[r^2 \exp\left\{-\left(\frac{2}{3B_x^2} + \frac{1}{3B_z^2}\right)r^2\right\} Y_{20}(\hat{r}) \phi(\alpha_1)\phi(\alpha_2)\right], \quad (4.4)$$

irrespectively of the deformation of its original intrinsic state. Therefore the overlap between spin-projected wave functions cannot become small but rather becomes close to unity as long as the values of $(2/B_x^2 + 1/B_z^2)$ are close to one another, irrespectively of the deformations of their intrinsic states. We can say that the essence of our above analysis is as follows: In the 2α system the spin-projected wave function is governed by a Gaussian-packet-like function $\chi_J(r)$ of a single coordinate r , the relative distance of the two α 's. Thus as long as one global character such as $\langle \chi_J | r^2 | \chi_J \rangle$ is similar, the spin-projected wave function can not differ so much, and there is no room for a difference with the original deformation. We see in summary that the origin of the seemingly strange results about the spin-projected wave functions comes from the simplicity or the smallness of the functional space of the 2α system. Hence this kind of things will not be possible to occur for 3α and heavier systems.

§5. Conclusion

In order to study non-zero-spin excitations of α -cluster condensation in the self conjugate $4n$ nuclei which we proposed in our previous paper, we introduced a spatial deformation into the α -cluster condensate. The wave function of the α -cluster condensate with deformation is obtained by a slight and natural modification of our previous wave function of the spherical condensate of α -clusters. As a first step and test case for the study of deformation, we, in this paper, investigated the ${}^8\text{Be}$ nucleus in applying the wave function of the deformed α -cluster condensate to the 2α -system. The 0^+ ground state, the 2^+ excited state at 2.9 MeV with $\Gamma_\alpha = 1.45$ MeV, and the 4^+ excited state at 11.4 MeV with $\Gamma_\alpha \approx 7$ MeV are known to constitute a rotational band whose intrinsic state has a 2α cluster structure with large inter- α distance. Our study in this paper gave us the following conclusions: (1) the spherical α -condensed wave function reproduces well the binding energy of the ground state, which implies that the 0^+ ground state can be considered as a 2α -particle quasi-bound state in relative s -wave with gas-like structure of dilute density. (2) The extension of the model space so as to include the deformed structure gives us only a slight energy gain of about 0.12 MeV for the 0^+ ground state. Corresponding to this small change of the binding energy, the change of the wave function due to the extension of the

model space is very small, although the deformed intrinsic wave function before the spin projection to $J = 0$ at the energy minimum is quite different from the spherical optimum wave function. Thus as far as the 0^+ ground state is concerned, the introduction of the deformed state plays essentially no role. (3) Our 0^+ wave function is found to be almost exactly equal to the 0^+ wave function obtained by the generator coordinate method using Brink's 2α wave function. This result strongly supports our new picture of the ^8Be structure that it is more a very dilute gas-like structure of 2α -particles rather than a dumb-bell structure of 2α -particles. (4) The deformed wave function reproduces well the observed excitation energy at 2.9 MeV of the 2^+ state. This result gives us the picture that not only the ground state but also the excited 2^+ state of ^8Be can be considered as a 2α -state with a gas-like structure of dilute density. This conclusion encourages us to introduce the deformed wave function of the α -condensation also for ^{12}C and heavier self-conjugate $4n$ nuclei for a future study of non-zero spin excitations of the α -condensation.

It is worth mentioning that our α -particle condensed wave function, introduced in Ref.[1], has so far reproduced quite accurately 0^+ -threshold states in ^{12}C and ^{16}O and the rotational states in ^8Be , treated in this paper. The fact that these results are obtained without a single adjustable parameter is, we believe, quite remarkable and gives strong credit to the correctness of the physics contained in our wave function.

Acknowledgements

One of the authors (Y. F.) would like to thank Dr. M. Kimura and Prof. Y. Fujiwara for helpful advices for the calculations.

Appendix A

— Matrix elements —

The deformed condensed wave function of Eq.(2.6) is written for the 2α system as

$$\Phi_{2\alpha}(\beta_x = \beta_y, \beta_z) = \int d^3 R_1 d^3 R_2 \exp\left(-\sum_{i=1}^2 \sum_{k=x,y,z} \frac{R_{ik}^2}{\beta_k^2}\right) \Phi^B(\mathbf{R}_1, \mathbf{R}_2). \quad (\text{A}\cdot 1)$$

By transforming \mathbf{R}_1 and \mathbf{R}_2 into the center-of-mass vector \mathbf{R}_G and the relative vector \mathbf{R} ,

$$\mathbf{R}_1 = \mathbf{R}_G + \frac{1}{2}\mathbf{R}, \quad \mathbf{R}_2 = \mathbf{R}_G - \frac{1}{2}\mathbf{R}, \quad (\text{A}\cdot 2)$$

this wave function is rewritten as

$$\begin{aligned} \Phi_{2\alpha}(\beta_x = \beta_y, \beta_z) &= 4! \left(\frac{4}{\pi b^2}\right)^{3/2} \int d^3 R_G \exp\left\{-\sum_{k=x,y,z} \frac{2}{\beta_k^2} R_{Gk}^2 - \frac{4}{b^2} (\mathbf{X}_G - \mathbf{R}_G)^2\right\} \\ &\times \int d^3 R \exp\left(-\sum_{k=x,y,z} \frac{1}{2\beta_k^2} R_k^2\right) \mathcal{A}\left[\exp\left\{-\frac{1}{b^2} (\mathbf{r} - \mathbf{R})^2\right\} \phi(\alpha_1) \phi(\alpha_2)\right], \end{aligned}$$

where $\mathbf{X}_G = (\mathbf{X}_1 + \mathbf{X}_2)/2$ and $\mathbf{r} = \mathbf{X}_1 - \mathbf{X}_2$, with \mathbf{X}_i denoting the center-of-mass coordinate of the i -th α cluster, α_i . Therefore the internal wave function,

$\widehat{\Phi}_{2\alpha}(\beta_x = \beta_y, \beta_z)$, of Eq.(2.11) is written as

$$\begin{aligned} \widehat{\Phi}_{2\alpha}(\beta_x = \beta_y, \beta_z) &= Q' \int d^3R \exp\left(-\sum_{k=x,y,z} \frac{1}{2\beta_k^2} R_k^2\right) \\ &\quad \times \mathcal{A} \left[\exp\left\{-\frac{1}{b^2}(\mathbf{r} - \mathbf{R})^2\right\} \phi(\alpha_1)\phi(\alpha_2) \right]. \end{aligned}$$

Now we introduce the following wave function, $\Psi_{2\alpha}(\beta_x = \beta_y, \beta_z)$,

$$\begin{aligned} \Psi_{2\alpha}(\beta_x = \beta_y, \beta_z) &= 4! \left(\frac{4}{\pi b^2}\right)^{3/2} \frac{1}{Q'} \exp\left(-\frac{4}{b^2} X_G^2\right) \widehat{\Phi}_{2\alpha}(\beta_x = \beta_y, \beta_z) \\ &= \int d^3R \exp\left(-\sum_{k=x,y,z} \frac{1}{2\beta_k^2} R_k^2\right) \Phi^B\left(\frac{1}{2}\mathbf{R}, -\frac{1}{2}\mathbf{R}\right). \end{aligned}$$

It is easy to prove the following relation

$$\begin{aligned} &\frac{\langle \widehat{\Phi}_{2\alpha}^J(\beta_x = \beta_y, \beta_z) | \widehat{O} | \widehat{\Phi}_{2\alpha}^J(\beta_x = \beta_y, \beta_z) \rangle}{\langle \widehat{\Phi}_{2\alpha}^J(\beta_x = \beta_y, \beta_z) | \widehat{\Phi}_{2\alpha}^J(\beta_x = \beta_y, \beta_z) \rangle} \\ &= \frac{\int d \cos \theta d_{00}^J(\theta) \langle \Psi_{2\alpha}(\beta_x = \beta_y, \beta_z) | \widehat{O} \widehat{R}_y(\theta) | \Psi_{2\alpha}(\beta_x = \beta_y, \beta_z) \rangle}{\int d \cos \theta d_{00}^J(\theta) \langle \Psi_{2\alpha}(\beta_x = \beta_y, \beta_z) | \widehat{R}_y(\theta) | \Psi_{2\alpha}(\beta_x = \beta_y, \beta_z) \rangle}. \end{aligned}$$

Below we give the explicit formulas of the matrix elements of the overlap, the kinetic energy, the two-body nuclear force, and the Coulomb force in the 2α system. We use below the notation $\Phi^B(\mathbf{R})$,

$$\Phi^B(\mathbf{R}) \equiv \Phi^B\left(\frac{1}{2}\mathbf{R}, -\frac{1}{2}\mathbf{R}\right). \quad (\text{A}\cdot 3)$$

The formula of the overlap is as follows.

$$\begin{aligned} &\langle \Psi_{2\alpha}(\beta_x = \beta_y, \beta_z) | \widehat{R}_y(\theta) | \Psi_{2\alpha}(\beta_x = \beta_y, \beta_z) \rangle \\ &= \int d^3S d^3R \exp\left\{-\sum_{k=x,y,z} \frac{S_k^2 + (R_y(\theta)\mathbf{R})_k^2}{2\beta_k^2}\right\} \langle \Phi^B(\mathbf{S}) | \Phi^B(\mathbf{R}) \rangle \\ &= (2\pi)^3 \beta_x^4 \beta_z^2 (G_0 + G_1 + G_2), \end{aligned}$$

$$\begin{aligned} G_0 &= \frac{2}{\sqrt{(2\alpha_1^2 + 1) \left\{ (2\alpha_1^2 + 1)(2\alpha_2^2 + 1) + \gamma \right\}}}, \\ G_1 &= -\frac{8}{\sqrt{\left(\frac{1}{2}\alpha_1^2 + 1\right) \left(\frac{3}{2}\alpha_1^2 + 1\right) \left\{ \left(\frac{1}{2}\alpha_1^2 + 1\right) \left(\frac{3}{2}\alpha_1^2 + 1\right) \left(\frac{1}{2}\alpha_2^2 + 1\right) \left(\frac{3}{2}\alpha_2^2 + 1\right) + \frac{\gamma}{4} \right\}}}, \\ G_2 &= \frac{6}{(\alpha_1^2 + 1)^2 (\alpha_2^2 + 1)}. \end{aligned}$$

In the above relation, we introduced variables, α_1 , α_2 , and γ , defined as

$$\alpha_1 \equiv \beta_x/b = \beta_y/b, \quad \alpha_2 \equiv \beta_z/b, \quad \gamma \equiv (\alpha_1^2 - \alpha_2^2)^2 \sin^2 \theta. \quad (\text{A}\cdot 4)$$

The formula of the kinetic energy is as follows.

$$\begin{aligned}
& \langle \Psi_{2\alpha}(\beta_x = \beta_y, \beta_z) | (T - T_G) \widehat{R}_y(\theta) | \Psi_{2\alpha}(\beta_x = \beta_y, \beta_z) \rangle \\
&= \int d^3 S d^3 R \exp \left\{ - \sum_{k=x,y,z} \frac{S_k^2 + (R_y(\theta) \mathbf{R})_k^2}{2\beta_k^2} \right\} \langle \Phi^B(\mathbf{S}) | T - T_G | \Phi^B(\mathbf{R}) \rangle \\
&= (2\pi)^3 \beta_x^4 \beta_z^2 \frac{\hbar^2}{mb^2} \left(\frac{21}{4} (G_0 + G_1 + G_2) \right. \\
&\quad \left. + \frac{G_0}{2} \left[\frac{3\alpha_1^2 + 1}{2\alpha_1^2 + 1} - \frac{\alpha_1^2 + \alpha_2^2 + 1}{(2\alpha_1^2 + 1)\{(2\alpha_1^2 + 1)(2\alpha_2^2 + 1) + \gamma\}} \right] \right. \\
&\quad \left. - \frac{G_1}{8} \left[\frac{(3\alpha_1^2 \alpha_2^2 - 4)(\frac{3}{4}\alpha_1^2 \alpha_2^2 + \alpha_1^2 + \alpha_2^2 + 1)}{(\frac{1}{2}\alpha_1^2 + 1)(\frac{3}{2}\alpha_1^2 + 1)(\frac{1}{2}\alpha_2^2 + 1)(\frac{3}{2}\alpha_2^2 + 1) + \frac{\gamma}{4}} + \frac{4(\frac{3}{2}\alpha_1^4 + 3\alpha_1^2 + 1)}{(\frac{1}{2}\alpha_1^2 + 1)(\frac{3}{2}\alpha_1^2 + 1)} \right] \right. \\
&\quad \left. - \frac{G_2}{2} \frac{2\alpha_1^2(\alpha_2^2 + 1) + \alpha_2^2(\alpha_1^2 + 1)}{(\alpha_1^2 + 1)(\alpha_2^2 + 1)} \right).
\end{aligned}$$

The formula of the two-body nuclear force is as follows.

$$\begin{aligned}
& \langle \Psi_{2\alpha}(\beta_x = \beta_y, \beta_z) | V_N \widehat{R}_y(\theta) | \Psi_{2\alpha}(\beta_x = \beta_y, \beta_z) \rangle \\
&= \int d^3 S d^3 R \exp \left\{ - \sum_{k=x,y,z} \frac{S_k^2 + (R_y(\theta) \mathbf{R})_k^2}{2\beta_k^2} \right\} \langle \Phi^B(\mathbf{S}) | V_N | \Phi^B(\mathbf{R}) \rangle \\
&= (2\pi)^3 \beta_x^4 \beta_z^2 \sum_{n=1}^2 v_n \left(\frac{a_n^2}{a_n^2 + 2b^2} \right)^{3/2} \\
&\times \left(4(X_d + X_e) \left(\frac{G_0}{2} + \frac{G_1}{4} + \frac{G_2}{6} \right) \right. \\
&\quad + \frac{4X_d}{\sqrt{(2\alpha_1^2 + 1)(u_n \alpha_1^2 + 1)\{(2\alpha_1^2 + 1)(u_n \alpha_1^2 + 1)(2\alpha_2^2 + 1)(u_n \alpha_2^2 + 1) + (u_n - 2)^2 \frac{\gamma}{4}\}}} \\
&\quad + \frac{4X_e}{\sqrt{(\frac{1}{2}\alpha_1^2 + 1)\{(u_n + \frac{3}{2})\alpha_1^2 + 1\} \left[(\frac{1}{2}\alpha_1^2 + 1)\{(u_n + \frac{3}{2})\alpha_1^2 + 1\}(\frac{1}{2}\alpha_2^2 + 1)\{(u_n + \frac{3}{2})\alpha_2^2 + 1\} + (u_n + 1)^2 \frac{\gamma}{4} \right]}} \\
&\quad + \frac{4(X_e - 2X_d)}{\sqrt{(\frac{3}{2}\alpha_1^2 + 1)\{(u_n + \frac{1}{2})\alpha_1^2 + 1\} \left[(\frac{3}{2}\alpha_1^2 + 1)\{(u_n + \frac{1}{2})\alpha_1^2 + 1\}(\frac{3}{2}\alpha_2^2 + 1)\{(u_n + \frac{1}{2})\alpha_2^2 + 1\} + (u_n - 1)^2 \frac{\gamma}{4} \right]}} \\
&\quad \left. - \frac{16(X_d + X_e)}{\sqrt{\left[(\alpha_1^2 + 1)\{(\frac{1}{2}u_n + 1)\alpha_1^2 + 1\} - \frac{\alpha_1^4}{4} \right] \left(\left[(\alpha_1^2 + 1)\{(\frac{1}{2}u_n + 1)\alpha_1^2 + 1\} - \frac{\alpha_1^4}{4} \right] \left[(\alpha_2^2 + 1)\{(\frac{1}{2}u_n + 1)\alpha_2^2 + 1\} - \frac{\alpha_2^4}{4} \right] + \frac{\gamma}{4} \right)}} \right)
\end{aligned}$$

$$\begin{aligned}
 & + \frac{4(X_d - 2X_e)}{\sqrt{(\alpha_1^2 + 1)\{(u_n + 1)\alpha_1^2 + 1\}[(\alpha_1^2 + 1)\{(u_n + 1)\alpha_1^2 + 1\}(\alpha_2^2 + 1)\{(u_n + 1)\alpha_2^2 + 1\} + u_n^2 \frac{\gamma}{4}]}} \\
 & + \frac{16(X_d + X_e)}{(\alpha_1^2 + 1)\{(\frac{1}{2}u_n + 1)\alpha_1^2 + 1\}\sqrt{(\alpha_2^2 + 1)\{(\frac{1}{2}u_n + 1)\alpha_2^2 + 1\}}} \Big).
 \end{aligned}$$

As explained in section §2.4, since we make use of the Volkov interaction as the two-body force, we should note that V_N reads as follows,

$$V_N = \frac{1}{2} \sum_{i \neq j}^8 \{(1 - M) - MP_\sigma P_\tau\}_{ij} \sum_{n=1}^2 v_n \exp\left(-\frac{r_{ij}^2}{a_n^2}\right).$$

In the above formula we used the variables defined below,

$$\begin{aligned}
 X_d &= 8 - 10M, \quad X_e = 10M - 2, \\
 u_n &= \frac{b^2}{a_n^2 + 2b^2}.
 \end{aligned}$$

As for the Coulomb force, we express it as a superposition of Gaussian functions which takes the form,

$$\begin{aligned}
 V_C &= \frac{1}{2} \sum_{i \neq j}^8 \frac{1 - \tau_{zi}}{2} \frac{1 - \tau_{zj}}{2} \frac{e^2}{r_{ij}} \\
 &= \frac{1}{2} \sum_{i \neq j}^8 \frac{1 - \tau_{zi}}{2} \frac{1 - \tau_{zj}}{2} \frac{2e^2}{\sqrt{\pi}} \int_0^\infty d\eta \exp(-r_{ij}^2 \eta^2).
 \end{aligned}$$

Therefore, we can easily obtain the matrix elements by changing the variables used in V_N in the following way,

$$\begin{aligned}
 a_n^2 &\longrightarrow \frac{1}{\eta^2}, \\
 \sum_{n=1}^2 v_n \left(\frac{a_n^2}{a_n^2 + 2b^2}\right)^{3/2} &\longrightarrow \frac{2e^2}{\sqrt{\pi}} \int_0^\infty \left(\frac{1}{1 + 2b^2\eta^2}\right)^{3/2} d\eta, \\
 X_d &\longrightarrow 2, \\
 X_e &\longrightarrow -1.
 \end{aligned}$$

It is convenient to change the integration variable from η to a new variable ξ defined as

$$\xi^2 = \frac{2b^2\eta^2}{1 + 2b^2\eta^2}, \quad \sqrt{\frac{1}{2b^2}} d\xi = \left(\frac{1}{1 + 2b^2\eta^2}\right)^{3/2} d\eta. \quad (\text{A}\cdot 5)$$

The range of integration over ξ is from zero to one. The numerical integration over ξ was performed by using the Gauss-Legendre method.

Appendix B

— Analytical calculation of spin projection —

Matrix elements with the angular-momentum-projected wave functions are obtained by integrating the formulas of Appendix A multiplied by $d_{00}^J(\theta)$ over the angle θ . We should note that in the formulas of Appendix A only $\gamma = (\alpha_1^2 - \alpha_2^2)^2 \sin^2 \theta$ depends on the angle θ . When limited to the case of 0^+ , 2^+ , and 4^+ , $d_{00}^J(\theta)$ contains only $\cos^2 \theta$ and $\cos^4 \theta$ as the terms which depend on θ . Therefore, the integrals for 0^+ , 2^+ , and 4^+ are classified into the following three types,

$$\begin{aligned} \int_{-1}^1 dx \frac{1}{\sqrt{A^2 - x^2}} &= 2 \arcsin\left(\frac{1}{A}\right), \\ \int_{-1}^1 dx \frac{x^2}{\sqrt{A^2 - x^2}} &= -\sqrt{A^2 - 1} + A^2 \arcsin\left(\frac{1}{A}\right), \\ \int_{-1}^1 dx \frac{x^4}{\sqrt{A^2 - x^2}} &= -\frac{1}{4}(2 + 3A^2)\sqrt{A^2 - 1} + \frac{3}{4}A^4 \arcsin\left(\frac{1}{A}\right), \end{aligned} \quad (\text{B}\cdot 1)$$

in the case of the overlap and nuclear force terms, and into the following three types,

$$\begin{aligned} \int_{-1}^1 dx \frac{1}{(A^2 - x^2)^{3/2}} &= \frac{2}{A^2 \sqrt{A^2 - 1}}, \\ \int_{-1}^1 dx \frac{x^2}{(A^2 - x^2)^{3/2}} &= \frac{2}{\sqrt{A^2 - 1}} - 2 \arcsin\left(\frac{1}{A}\right), \\ \int_{-1}^1 dx \frac{x^4}{(A^2 - x^2)^{3/2}} &= \sqrt{A^2 - 1} + \frac{2A^2}{\sqrt{A^2 - 1}} - 3A^2 \arcsin\left(\frac{1}{A}\right), \end{aligned} \quad (\text{B}\cdot 2)$$

in the case of the kinetic terms. Here $x = \cos \theta$ and we note that A always takes values more than unity.

Appendix C

— Limit of $\beta_x \rightarrow \beta_z$ for spin projected states —

We stated in §2.3, that there exist non-zero spin states on the $\beta_x (= \beta_y) = \beta_z$ line. They are defined by the limiting procedure of $\beta_x \rightarrow \beta_z$. We can obtain the matrix elements with these limiting states analytically by performing Taylor expansion with respect to $s \equiv \alpha_1^2 - \alpha_2^2$ around $s = 0$. In this appendix, we display the series expansions with respect to s up to the second order for the case of the 2^+ state. For the sake of the series expansion, we introduce $t \equiv \alpha_1^2 + \alpha_2^2$ and rewrite α_1^2 and α_2^2 by s and t as

$$\alpha_1^2 = \frac{1}{2}(s + t), \quad \alpha_2^2 = \frac{1}{2}(t - s). \quad (\text{C}\cdot 1)$$

By using

$$d_{00}^2(x) = \frac{3}{2}x^2 - \frac{1}{2}, \quad (\text{C}\cdot 2)$$

we get the series expansions about the overlap terms as follows,

$$\widehat{G}_0 = \int_{-1}^1 dx \left(\frac{3}{2}x^2 - \frac{1}{2} \right) G_0 = \frac{4}{15} \frac{1}{(t+1)^{7/2}} s^2 - \frac{2}{15} \frac{1}{(t+1)^{9/2}} s^3 + \dots,$$

$$\begin{aligned}
 \widehat{G}_1 &= \int_{-1}^1 dx \left(\frac{3}{2}x^2 - \frac{1}{2} \right) G_1 = -\frac{4}{15} \frac{1}{\left\{ \left(\frac{1}{4}t + 1 \right) \left(\frac{3}{4}t + 1 \right) \right\}^{7/2}} s^2 \\
 &\quad + \frac{1}{30} \frac{\frac{3}{2}t + 4}{\left\{ \left(\frac{1}{4}t + 1 \right) \left(\frac{3}{4}t + 1 \right) \right\}^{9/2}} s^3 - \dots, \\
 \widehat{G}_2 &= \int_{-1}^1 dx \left(\frac{3}{2}x^2 - \frac{1}{2} \right) G_2 = 0.
 \end{aligned} \tag{C.3}$$

About the kinetic terms, we get

$$\begin{aligned}
 &\int_{-1}^1 dx \left(\frac{3}{2}x^2 - \frac{1}{2} \right) \langle \Psi_{2\alpha}(\beta_x = \beta_y, \beta_z) | (T - T_G) \widehat{R}_y(x) | \Psi_{2\alpha}(\beta_x = \beta_y, \beta_z) \rangle \\
 &= (2\pi)^3 \beta_x^4 \beta_z^2 \frac{\hbar^2}{mb^2} \left[\frac{21}{4} (\widehat{G}_0 + \widehat{G}_1 + \widehat{G}_2) \right. \\
 &\quad - \frac{1}{15} \frac{3t - 4}{(t + 1)^{9/2}} s^2 + \frac{1}{10} \frac{t - 2}{(t + 1)^{11/2}} s^3 + \dots \\
 &\quad + \frac{1}{120} \frac{15t^2 + 24t - 32}{\left\{ \left(\frac{3}{4}t + 1 \right) \left(\frac{1}{4}t + 1 \right) \right\}^{9/2}} s^2 - \frac{1}{640} \frac{15t^3 + 56t^2 - 128}{\left\{ \left(\frac{3}{4}t + 1 \right) \left(\frac{1}{4}t + 1 \right) \right\}^{11/2}} s^3 + \dots \\
 &\quad \left. - 0 \right].
 \end{aligned} \tag{C.4}$$

About the terms which come from the nuclear force, we have

$$\begin{aligned}
 &\int_{-1}^1 \left(\frac{3}{2}x^2 - \frac{1}{2} \right) \langle \Psi_{2\alpha}(\beta_x = \beta_y, \beta_z) | V_N \widehat{R}_y(x) | \Psi_{2\alpha}(\beta_x = \beta_y, \beta_z) \rangle \\
 &= (2\pi)^3 \beta_x^4 \beta_z^2 \sum_{n=1}^2 v_n \left(\frac{a_n^2}{a_n^2 + 2b^2} \right)^{3/2} \\
 &\quad \left\{ 4(X_d + X_e) \left(\frac{\widehat{G}_0}{2} + \frac{\widehat{G}_1}{4} + \frac{\widehat{G}_2}{6} \right) \right. \\
 &\quad + 4X_d \left(\frac{4}{15} \frac{\sqrt{2}(u_n - 2)^2}{\left\{ (t + 1)(u_n t + 2) \right\}^{7/2}} s^2 - \frac{2}{15} \frac{\sqrt{2}(u_n - 2)^2 (2u_n t + u + 2)}{\left\{ (t + 1)(u_n t + 2) \right\}^{9/2}} s^3 + \dots \right) \\
 &\quad + 4X_e \left(\frac{1}{30} \frac{(u_n + 1)^2}{\left\{ \left(\frac{1}{4}t + 1 \right) \left(\frac{2u_n + 3}{4}t + 1 \right) \right\}^{7/2}} s^2 - \frac{1}{120} \frac{(u_n + 1)^2 \left(\frac{2u_n + 3}{4}t + u_n + 2 \right)}{\left\{ \left(\frac{1}{4}t + 1 \right) \left(\frac{2u_n + 3}{4}t + 1 \right) \right\}^{9/2}} s^3 + \dots \right) \\
 &\quad + 4(X_e - 2X_d) \left(\frac{1}{30} \frac{(u_n - 1)^2}{\left\{ \left(\frac{3}{4}t + 1 \right) \left(\frac{2u_n + 1}{4}t + 1 \right) \right\}^{7/2}} s^2 - \frac{1}{120} \frac{(u_n - 1)^2 \left(\frac{6u_n + 3}{4}t + u_n + 2 \right)}{\left\{ \left(\frac{3}{4}t + 1 \right) \left(\frac{2u_n + 1}{4}t + 1 \right) \right\}^{9/2}} s^3 + \dots \right) \\
 &\quad \left. - 16(X_d + X_e) \left(\frac{1}{30} \frac{1}{\left(\frac{2u_n + 3}{16}t^2 + \frac{u_n + 4}{4}t + 1 \right)^{7/2}} s^2 - \frac{1}{120} \frac{\frac{2u_n + 3}{4}t + \frac{u_n}{2} + 2}{\left(\frac{2u_n + 3}{16}t^2 + \frac{u_n + 4}{4}t + 1 \right)^{9/2}} s^3 + \dots \right) \right\}
 \end{aligned}$$

$$\begin{aligned}
& +4(X_d - 2X_e) \left(\frac{64}{15} \frac{u_n^2}{[(t+2)\{(u_n+1)t+2\}]^{7/2}} s^2 - \frac{64}{15} \frac{\{(u_n+1)t+u_n+2\}u_n^2}{[(t+2)\{(u_n+1)t+2\}]^{9/2}} s^3 + \dots \right) \\
& +16(X_d + X_e) \times 0 \left. \vphantom{\frac{64}{15}} \right\}. \tag{C.5}
\end{aligned}$$

References

- [1] A. Tohsaki, H. Horiuchi, P. Schuck, and G. Röpke, Phys. Rev. Letters **87**, 192501 (2001).
- [2] F. Ajzenberg-Selove, Nucl. Phys. **A460**, 1 (1986).
- [3] Y. Fujiwara, H. Horiuchi, K. Ikeda, M. Kamimura, K. Kato, Y. Suzuki, and E. Uegaki, Prog. Theor. Phys. Supplement No.68, 29 (1980).
- [4] A. D. Bacher, F. G. Resmini, H. E. Conzett, R. de Swiniarski, H. Meiner, and J. Ernst, Phys. Rev. Letters **29**, 1331 (1972).
- [5] A. B. Volkov, Nucl. Phys. **74**, 33 (1965).
- [6] A. Tohsaki, Phys. Rev. C **49**, 1814 (1994).
- [7] U. Lombardo and P. Schuck, Phys. Rev. C **63**, 038201 (2001).
- [8] F. Tanabe, A. Tohsaki, and R. Tamagaki, Prog. Theor. Phys. **53**, 677 (1975).

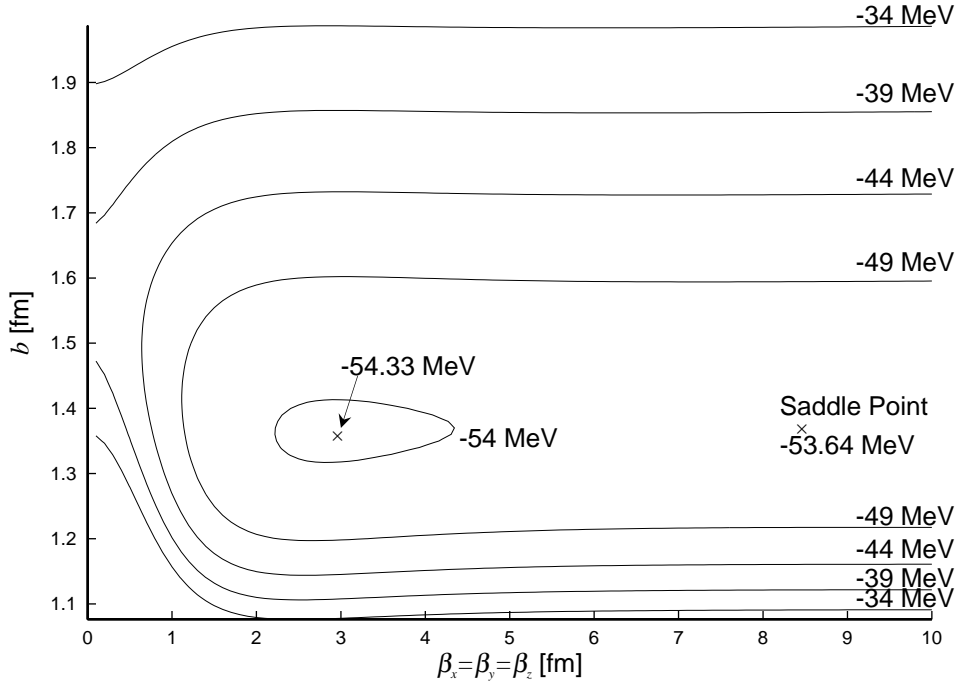


Fig.1: Contour map of the energy surface of the spherical state for $M = 0.56$ in the two parameter space, b and $\beta_x = \beta_y = \beta_z$.

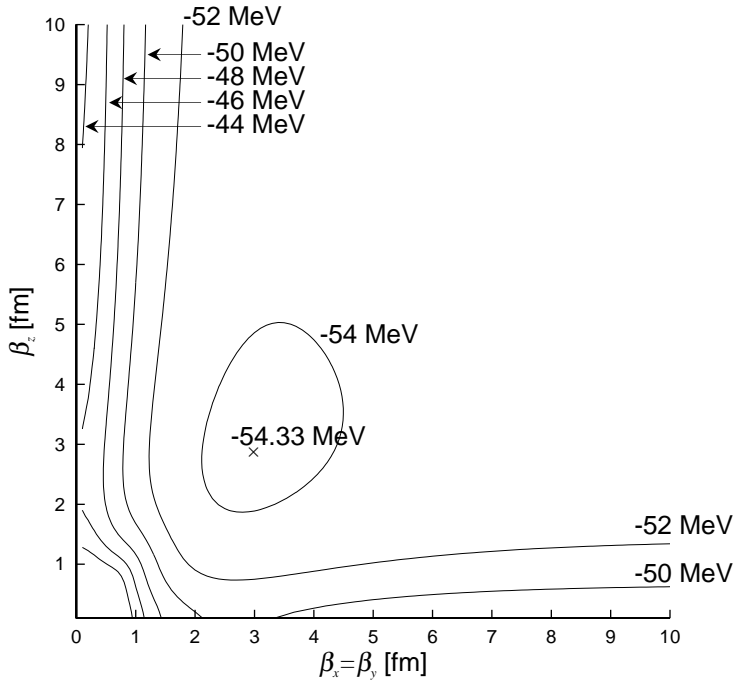


Fig.2: Contour map of the energy surface of the deformed intrinsic state for $M = 0.56$ in the two parameter space, $\beta_x (= \beta_y)$ and β_z .

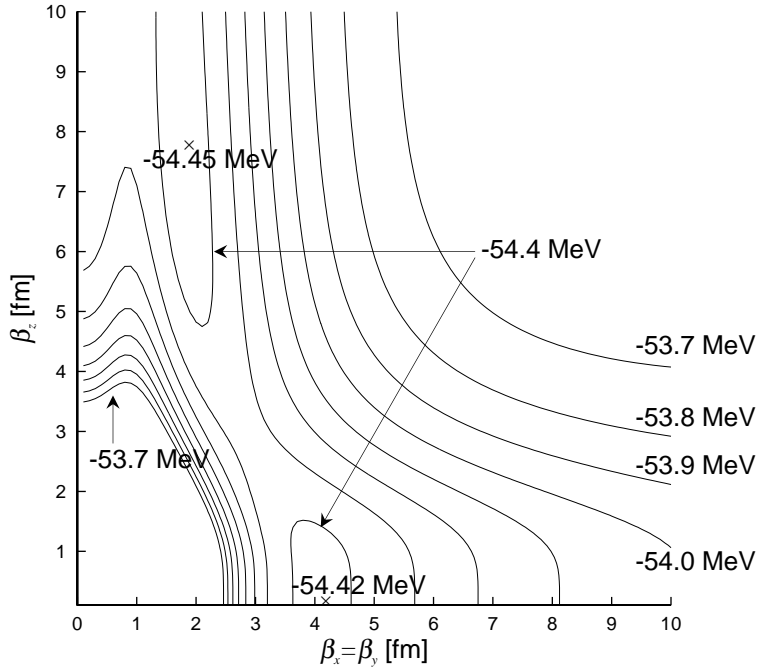


Fig.3: Contour map of the energy surface of the 0^+ state for $M = 0.56$ in the two parameter space, $\beta_x (= \beta_y)$ and β_z .

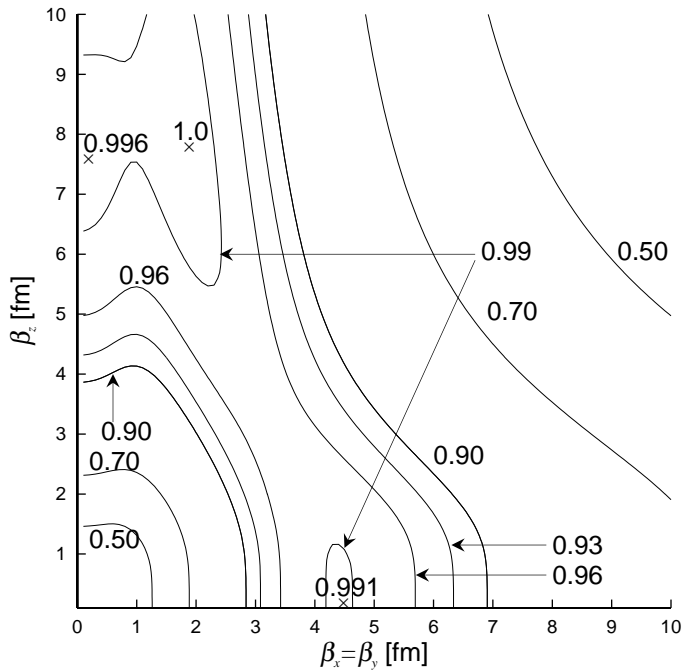


Fig.4(a): Contour map of the squared overlap $O(\beta_x, \beta_z)$ between the 0^+ wave function with $\beta_x = \beta_y = 1.8$ fm, $\beta_z = 7.8$ fm and the 0^+ wave function with variable $\beta_x (= \beta_y)$ and β_z . Numbers attached to the contour lines are squared overlap values.

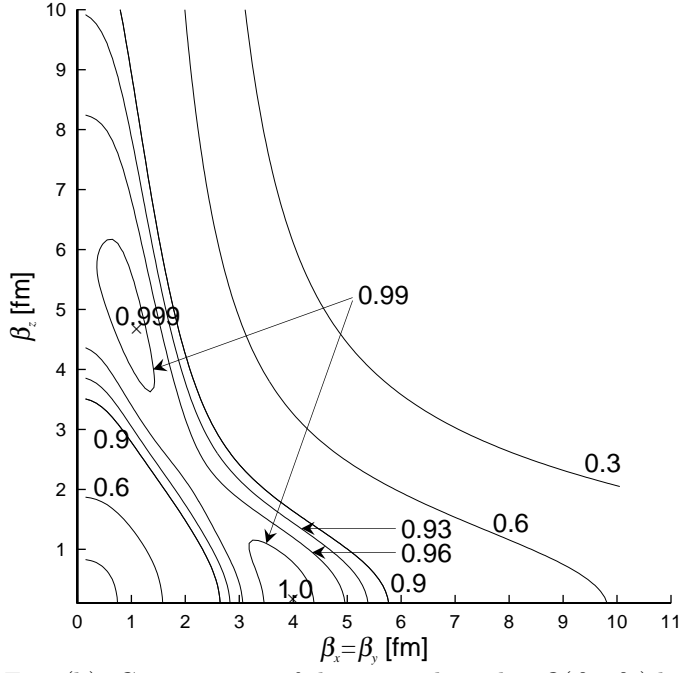


Fig.4(b): Contour map of the squared overlap $O(\beta_x, \beta_z)$ between the 2^+ wave function with $\beta_x = \beta_y = 3.9$ fm, $\beta_z = 0.0$ fm and the 2^+ wave function with variable $\beta_x (= \beta_y)$ and β_z . Numbers attached to the contour lines are squared overlap values.

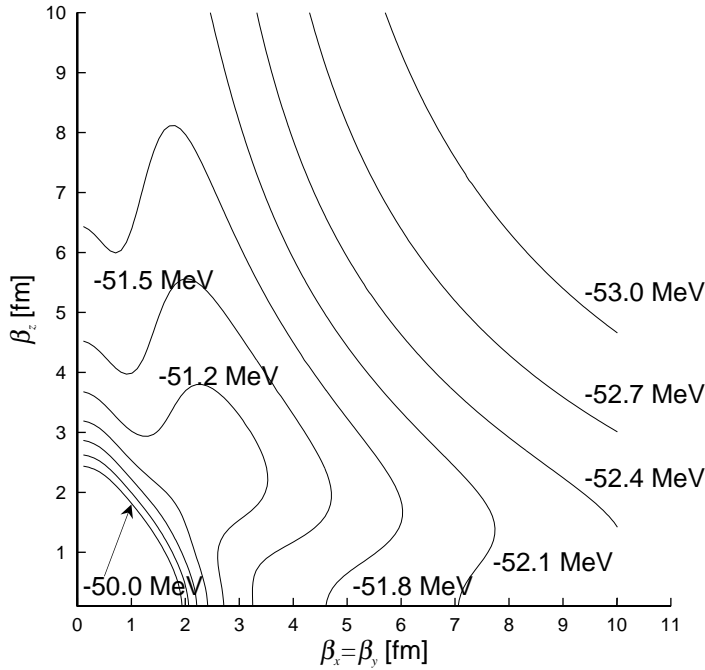


Fig.5: Contour map of the energy surface of the 2^+ state for $M = 0.56$ in the two parameter space, $\beta_x (= \beta_y)$ and β_z .

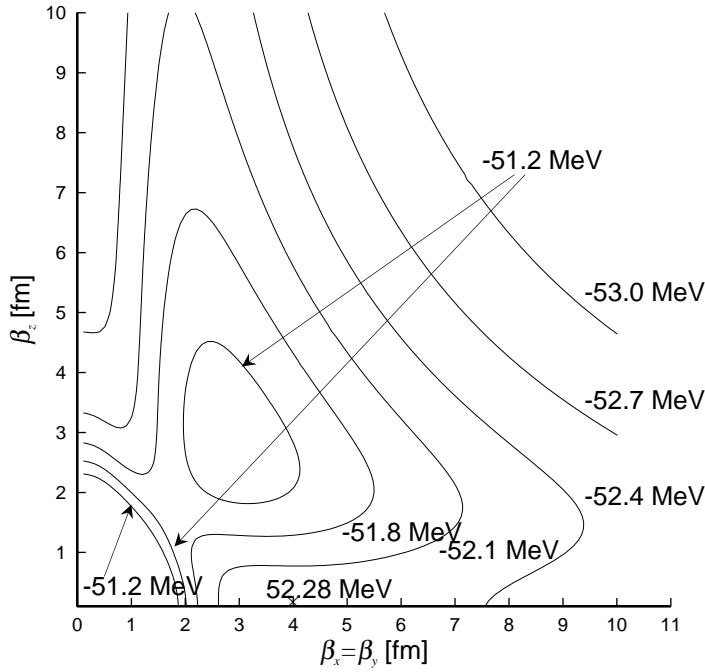


Fig.6: Contour map of the energy surface of the 2^+ state for $M = 0.54$ in the two parameter space, $\beta_x (= \beta_y)$ and β_z .

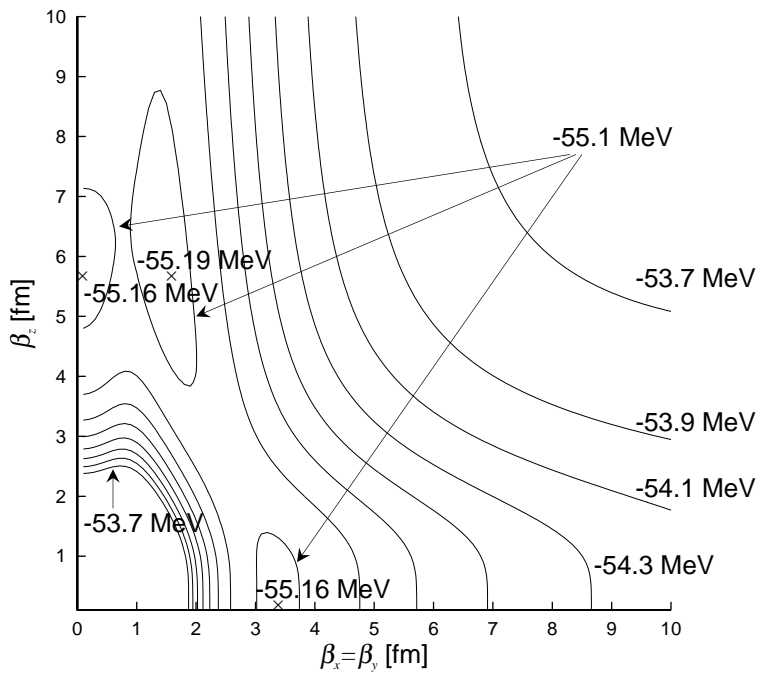


Fig.7: Contour map of the energy surface of the 0^+ state for $M = 0.54$ in the two parameter space, $\beta_x (= \beta_y)$ and β_z .

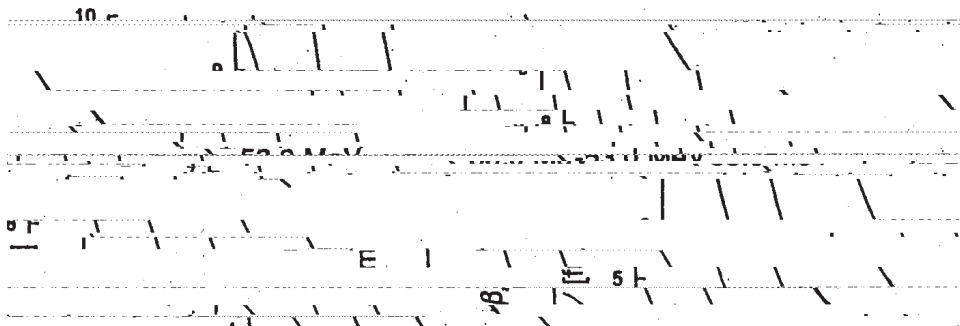


Fig.8: Contour map of the energy surface of the 4^+ state for $M = 0.56$ in the two parameter space, $\beta_x(= \beta_y)$ and β_z .

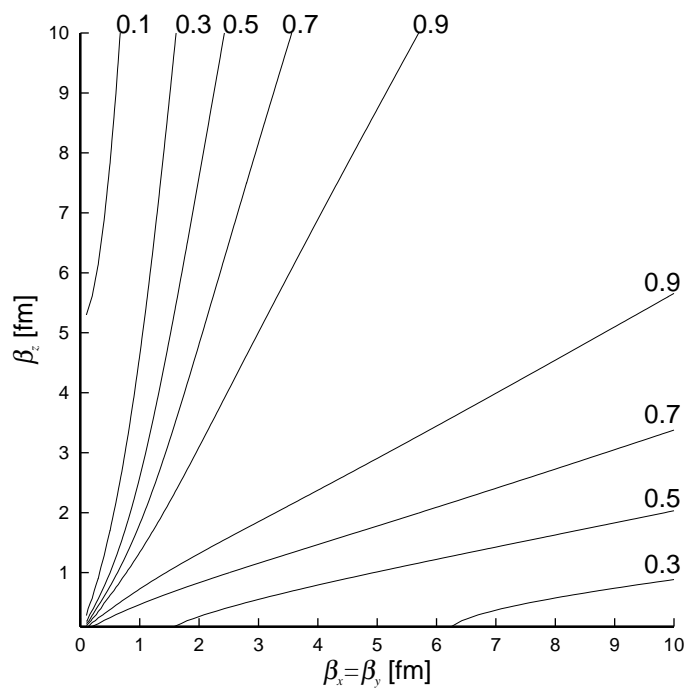


Fig.9(a): Contour map of the squared amplitude of J^+ component contained in the deformed wave function in the two parameter space, $\beta_x(= \beta_y)$ and β_z for $J = 0$.

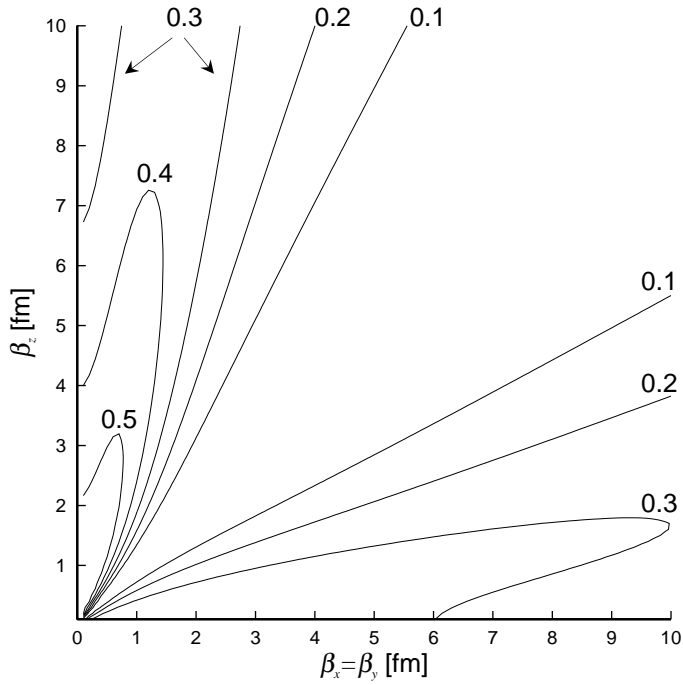


Fig.9(b): Contour map of the squared amplitude of J^+ component contained in the deformed wave function in the two parameter space, $\beta_x(=\beta_y)$ and β_z for $J = 2$.

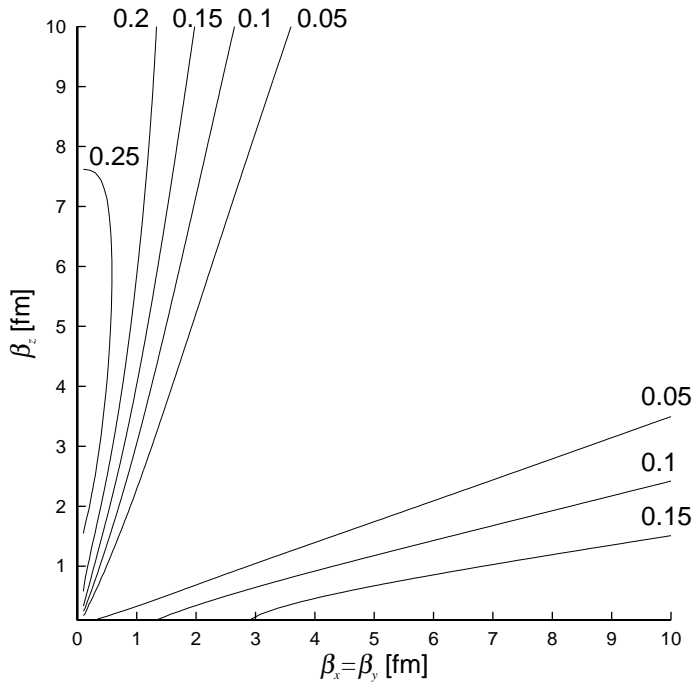


Fig.9(c): Contour map of the squared amplitude of J^+ component contained in the deformed wave function in the two parameter space, $\beta_x(=\beta_y)$ and β_z for $J = 4$.

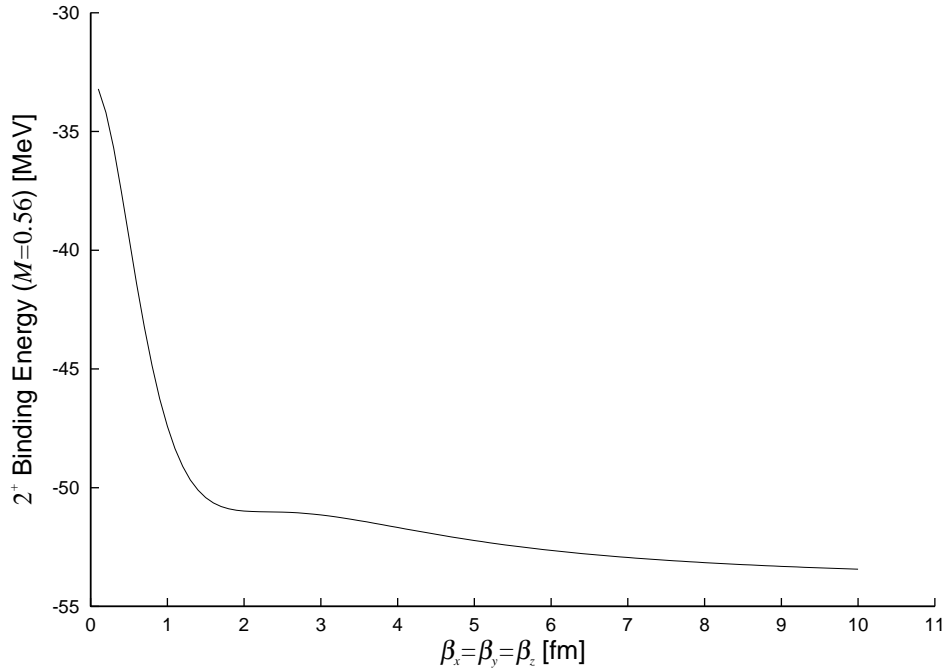


Fig.10: Binding energy of the 2^+ state on the $\beta_x = \beta_y = \beta_z$ line.

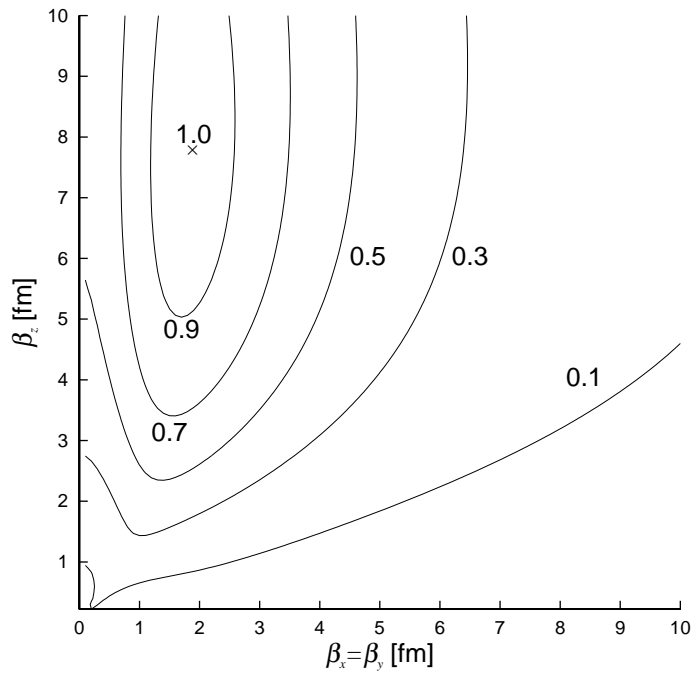


Fig.11: Contour map of the squared overlap between the prolate intrinsic wave function with $\beta_x = \beta_y = 1.8$ fm, $\beta_z = 7.8$ fm and the intrinsic wave function with variable $\beta_x (= \beta_y)$ and β_z .